Available online at www.sciencedirect.com
SCIENCE DIRECT®
International Journal of Mass Spectrometry 241 (2005) 119–132
International Journal of Mass Spectrometry
www.elsevier.com/locate/ijms

Geometry optimization for the cylindrical ion trap: field calculations, simulations and experiments

Guangxiang Wu, R. Graham Cooks*, Zheng Ouyang*

Department of Chemistry, Purdue University, West Lafayette, IN 47907-2084, USA

Received 7 November 2004; accepted 1 December 2004
Available online 8 January 2005

Dedicated to Bill Hase with admiration and best wishes on the occasion of his 60th birthday.

Abstract

Optimization of ion trap geometries for best analytical performance was studied in the specific case of the cylindrical ion trap (CIT). An optimization procedure was developed based on field calculations and simulations of ion motion. The electric field inside the CIT was calculated by using the Poisson/Superfish software package and geometrical effects, specifically the half thickness of the ring electrode (z_b), the spacing (d_s) between the ring electrode and the end-cap electrode, and the end-cap hole radius (r_H), were systematically investigated. Appropriate compensation for higher-order field components, namely octapolar and dodecapolar fields, was achieved by refining the CIT geometry and improved mass resolution in scans using boundary and resonance ejection. Resolution for different CIT geometries was measured in both simulations and experiments and was evaluated from the separation between the major isotope peaks of 1,3-dichlorobenzene at *m/z* 146 and 148. Optimization of the CIT electric field via simple geometry changes involved exploration of several geometries and simulations using the ion trap simulation program (ITSIM) were used to confirm the results for each geometry and to predict experimental performance. Experiments are reported that confirm the enhanced performance achieved using the CITs optimized using the procedure developed in this study.

Keywords: Ion trap mass spectrometer; Higher-order fields; Ion trap simulation; Non-linear resonance

1. Introduction

Mass spectrometry is widely used due to its high specificity and high sensitivity. The broad range of applications of mass spectrometry indicates that the functional requirements of a mass spectrometer vary significantly according to the specific application. The development of mass spectrometers is advancing, on the one hand, towards high performance instrumentation with high mass range, high mass resolution and high mass accuracy, especially for applications in the life sciences. On the other hand, miniaturization of mass spectrometry instruments is actively being pursued to provide tools for fieldable chemical analysis [1–5]. The strategy pursued in the development of these small mass spectrometers has been to achieve adequate analytical performance with instruments of reduced size, weight and power consumption.

Miniaturization of the mass spectrometer involves using a smaller mass analyzer [6], a lower electric or magnetic field strength for the smaller analyzer to retain the mass range [7–9], and the minimum vacuum pumping capability needed to avoid excessive collisions between ions and neutral molecules [10,11]. Miniaturization has been attempted with numerous types of mass analyzers [6]. In some instances, the geometries of the miniature mass analyzers have also been simplified to avoid difficulty in mechanical fabrication at smaller scales. The sensitivity of analysis using miniature mass analyzers has not been found to be significantly compromised [12–14]. However, the mass resolution of a miniature mass analyzer is determined in large part by the extent of optimization of its simplified geometry [15,16]. An

* Corresponding authors. Tel.: +1 765 494 5262 (R.G. Cooks)/ +1 765 496 1539 (Z. Ouyang);
fax: +1 765 494 0239 (R.G. Cooks)/+1 765 494 9421 (Z. Ouyang).
E-mail addresses: cooks@purdue.edu (R.G. Cooks), ouyang@purdue.edu (Z. Ouyang).

1387-3806/$ – see front matter © 2004 Elsevier B.V. All rights reserved.
doi:10.1016/j.ijms.2004.12.004

adequate mass resolution under given conditions, limited by the vacuum restriction imposed by the compromised pumping capability of a small mass spectrometer, has been the decisive factor for the success of miniaturization.

One mass analyzer which has been miniaturized for fieldable instruments, the cylindrical ion trap (CIT), was originally used as an ion storage device [17], then developed as a mass analyzer [18], miniaturized to smaller sizes [9,13,19], and then implemented in a portable ion trap mass spectrometer [14,20]. A large amount of effort has been expended on the optimization of the CIT geometry to achieve unit or better mass resolution [13,15,16,18]. Although a new geometry ion trap, the rectilinear ion trap (RIT), has been recently demonstrated to provide improved sensitivity [21], the CIT remains easier to fabricate, miniaturize and multiplex [15,19,22], and it represents the only simplified geometry ion trap to be commercialized.

Since Dawson performed the first ion calculations of ion motion in a quadrupole field [23], numerical simulations have been demonstrated as an effective approach to explore ion trajectories. This has been done under varying conditions which include non-linear fields and under the influence of resonance excitation [24–30]. Simulations have also proven to be a very useful tool to facilitate instrumentation development, as in the case of the linear quadrupole mass filter and the digital ion trap mass spectrometer [31,32]. Use of simulations to optimize analytical performance has been briefly described previously [33–35]. Here, the ion trap simulation program ITSIM [26,33,36] was adapted to allow the calculation of the trapping field, the simulation of the ion trajectories, and the prediction of mass spectra using CITs of a specific geometries. Experimental tests have been carried out in parallel with the simulations and the results from both simulations and experiments were correlated to facilitate the design of improved CITs. After years of improvement of the ITSIM program and its application to the CIT, experience has been accumulated and the method of using the field calculation and ion trajectory simulation for the CIT optimization has become mature [13,15,18,33]. However, without a procedure that is easy to follow, successful optimization still requires detailed understanding of ion trap theory and prior-experience with the CIT. In this paper, we introduce a CIT optimization procedure that can easily be followed. This procedure involves the field calculation, ion trap simulation, and an important empirical rule that will be explained in detail.

2. Experimental

The CIT geometry is shown in Fig. 1. It consists of a symmetrically placed cylindrical ring electrode and two planar end-cap electrodes. Five CIT geometries with ring electrode radius $r_0 = 5.0$ mm were used in this study to help illustrate the process of CIT optimization, and these geometries are

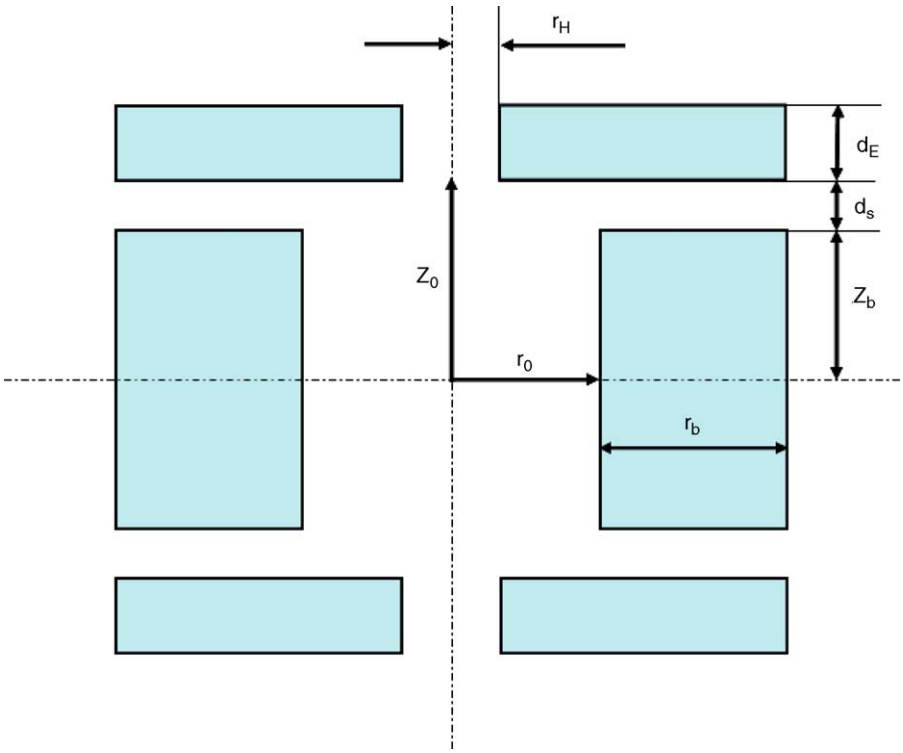

Fig. 1. Parameters used to describe CIT geometry: the center-to-end-cap distance ($z_0 = z_b + d_s$), half thickness of the ring electrode (z_b), inner radius of the ring electrode (r_0), thickness of the ring electrode in the radial direction (r_b), end-cap hole radius (r_H), the spacer between the ring electrode and the endcap (d_s) and the thickness of the endcap (d_E).

Table 1
Dimensions for different CITs with $r_0 = 5.0$ mm, $r_b = 4.5$ mm and $d_E = 0.3$ mm

CIT	z_0 (mm)	z_b (mm)	d_s (mm)	r_H (mm)
CIT-0	5.0	3.4	1.6	0.5
CIT-1	5.0	3.4	1.6	1.5
CIT-2	5.3	3.7	1.6	1.5
CIT-3	5.5	3.4	2.1	1.5
CIT-4	5.0	4.3	0.7	1.5

listed in Table 1. They differ only in the dimensions of z_0 ($z_0 = z_b + d_s$), z_b, d_s and r_H. The internal electric field of a CIT to be optimized was first calculated and then adjusted by varying the above geometrical parameters. The performance of the CIT was predicted by simulation and confirmed by the experimental results.

2.1. Field calculations

The electric field inside the CIT was calculated using the home-written program CreatePot, which uses the program Poisson from the Poisson/Superfish package (Los Alamos National Laboratory, Los Alamos, NM) [37] to solve the Laplace equation. CreatePot creates a geometry input file for Poisson and automatically calls the Poisson Laplace solver. The Poisson program covers a region of space within specified boundaries with a triangular mesh and calculates the potential at each point of the mesh. The potential values are exported to CreatePot, and a least-square fit is then used to calculate the multipole expansion coefficients representing the field strength.

2.2. Simulations

The mass spectra predicted for different CIT geometries were simulated by using the ion trap trajectory simulation program ITSIM 5.0 (Purdue University, West Lafayette, IN) [33,36]. ITSIM is a Microsoft Windows based program specifically developed to study the behavior of collections of ions in ion traps. It allows the motion of a large number of ions inside the CIT to be followed under user-defined experimental conditions. The ions are generated in the trap with selected spatial and velocity distributions and different mass/charge ratios. The electric field is calculated by interpolation from an array of electric potential values extracted from the Poisson solution. The ion trajectories are calculated numerically by solving Newton's equation of motion with Runge–Kutta methods [38]. Elastic and inelastic ion–neutral interactions and ion–ion space charge effects are also implemented with the ITSIM package.

2.3. Experimental verification

The performance of five CITs with different geometries was tested in a system that used the control electronics and vacuum system of a prototype Thermo Finnigan ITMS [39]. The instrumental setup is shown in Fig. 2. The original quadrupole ion trap inside the vacuum manifold was replaced with a cylindrical ion trap for these experiments. The CIT ring electrodes were machined from 304 stainless-steel and the inner radius was held constant at 5.0 mm. The planar endcaps (0.3 mm in thickness) were machined from thin stainless-steel with a center hole radius $r_H = 0.5$ or 1.5 mm and were separated from the ring electrode by Delrin spacers

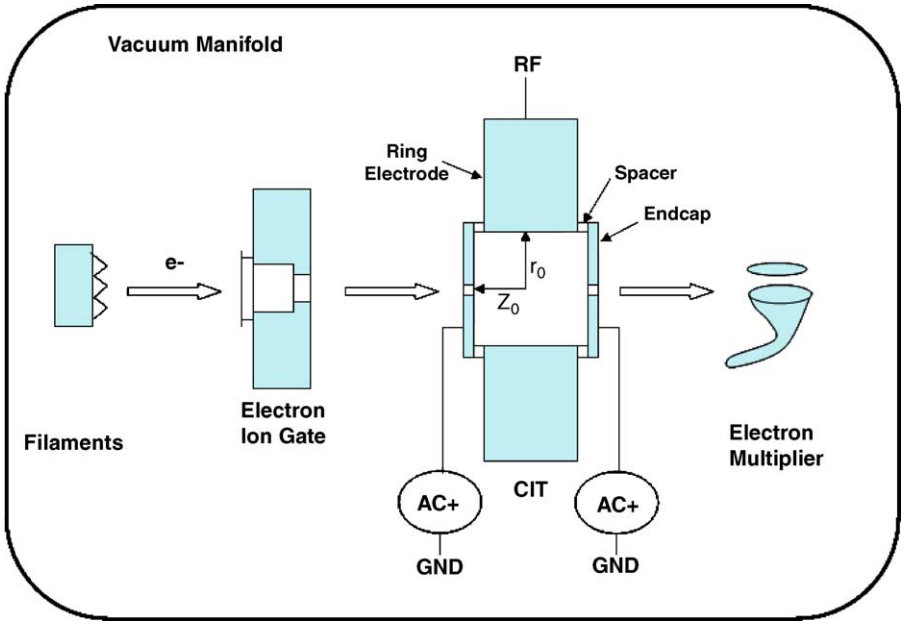

Fig. 2. Experimental system used for the experiments. CIT has inner radius $r_0 = 5.0$ mm. An rf signal is applied to the ring electrode, while the endcaps are either grounded for boundary ejection or supplied with a dipolar ac signal with 180° phase difference for resonance ejection.

(The Dupont Co., Wilmington, DE). An RF signal (1.1 MHz) was applied to the ring electrode and the end-cap electrodes were grounded during boundary ejection. In the case of resonance ejection, an extra ac signal was generated using a waveform generator (Wavetek 395, San Diego, CA, USA) and applied in the dipolar mode with 180° phase difference to the end-cap electrodes using a Balun amplifier. Trapped ions were mass selectively ejected by scanning the rf amplitude at a rate of 68 V/ms, corresponding to a scan rate of 18 Th/ms. Internal electron ionization was used to ionize neutral molecules inside the CIT, and an electron gating lens was used to control the time during which electrons from a heated filament were allowed to enter the CIT through the end-cap hole. During the experiments, the ionization time was controlled to limit the number of ions created inside the trap and thus to avoid undesirable space charge effects [40]. The ions ejected from the CIT were detected using an electron multiplier which was operated at −1800 V with a conversion dynode operated at −5 kV. The ion signal was first amplified using the preamplifier in the ITMS and then acquired using a digital oscilloscope (Model TDS 540; Tektronix Beaverton, OR, USA) at a sampling rate of 250 K samples/s.

The compound 1,3-dichlorobenzene (Aldrich Chemical Co., Inc.) was leaked into the manifold to an indicated pressure of ca. 8×10^{-7} Torr. The vapor was introduced using a Granville–Phillips (Granville–Phillips Co., Boulder, CO, USA) leak valve after one freeze-pump-thaw cycle. Helium buffer gas was then added to an indicated manifold pressure of ca. 8×10^{-5} Torr. The uncorrected sample and helium pressure readings were made using a Bayert–Alpert ionization gauge with a Granville–Phillips 307 vacuum controller (Granville–Phillips, Boulder, CO).

To compare the experimental resolution of the CITs with the mass spectra obtained via simulations, the extent of the separation between the isotope peaks at *m*/*z* 146 and 148 in the mass spectrum of 1,3-dichlorobenzene was used, as measured by the percentage of the valley between *m*/*z* 146 and 148. The ratio of the height of the valley to the average height of the peaks at *m*/*z* 146 and 148 was compared for the five different CIT geometries.

3. Results and discussion

As shown in Fig. 1, the cylindrical ion trap consists of a ring electrode and planar end-cap electrodes, characteristics which differentiate it from conventional Paul traps with the hyperbolic electrode surfaces. As a type of quadrupole ion trap, ion motion in the CIT is driven by (a) the main rf electric field, (b) the dipolar auxiliary ac field, (c) collisions with neutral molecules, and (d) the columbic forces between the ions. Optimum conditions with respect to collision and columbic effects are usually achieved by adjusting the internal buffer gas pressure in addition to the number of trapped ions, the latter being directly controlled by the ionization time [27]. The optimum electric field, affected both by the main rf and the dipolar auxiliary ac, is a function of the CIT geometry. These interrelationships form the main subject of this study of CIT performance optimization.

3.1. Electric field in the CIT and optimum conditions for mass resolution

The electric potential at any point in the ion trap is given by the solution to the Laplace equation [41]. For the cylindrical ion trap, Benilan and Audoin [42] and Bonner et al. [43] have shown that the electric potential can be expressed analytically by Bessel functions. In the particular case where the potential V_{ring} is applied to the ring electrode with both end-caps grounded, the potential can be expressed in cylindrical coordinates (*r*,*z*) [44]:

$$\Phi(r, z) = 1 - 2\sum_{j=1}^{\infty} \frac{\cosh(x_j z) J_0(x_j r)}{x_j \cosh(x_j z_0) J_1(x_j r_0)} \tag{1}$$

where J_0 and J_1 are Bessel functions of the first kind and $x_j r_0$ the *j*th zero of $J_0(x)$. It is convenient to expand the potential in spherical harmonics including terms of a multipole expansion, which is the sum of the various field components superimposed upon one another and described by the weights given to the each of the field components. In cylindrical polar coordinates (*r*,*φ*,*z*), one obtains:

$$\Phi(r, z, \phi) = \Phi_0 \left[A_0 + \frac{A_1}{r_N} z + \frac{A_2}{r_N^2} \left(\frac{1}{2} r^2 - z^2 \right) + \frac{A_3}{r_N^3} \left(\frac{3}{2} r^2 z - z^3 \right) + \frac{A_4}{r_N^4} \left(\frac{3}{8} r^4 - 3 r^2 z^2 + z^4 \right) + \cdots \right] \tag{2}$$

where Φ_0 is the potential applied to the ring electrode, and r_N the normalization radius which is chosen to be r_0. The terms that involve the angular coordinates do not appear in Eq. (2) due to the cylindrical symmetry of the CIT trap. The term A_n is the dimensionless expansion coefficient of order *n*, and the values of the terms for $n = 0$–4 correspond to monopole, dipole, quadrupole, hexapole and octapole electric field contributions, respectively. The monopole term A_0 does not contribute to the electric field and can be ignored. Also for the cylindrical ion trap having reflection symmetry with respect to the central *x*–*y* plane, the dipole term A_1 and all higher odd order terms also disappear. The even coefficients are given by [45]:

$$A_{2n} = \frac{2}{(2n)!} \sum_{j=1}^{\infty} \frac{\left(x_j r_0\right)^{2n-1}}{\cosh\left(x_j z_0\right) J_1\left(x_j r_0\right)} + \delta_{n,0} \tag{3}$$

where $\delta_{n,0}$ is unity if $n = 0$, and otherwise is zero. Among all the multipole expansion coefficients, the quadrupolar field (A_2) and two other higher-order field components, the octap-

olar field (A_4) and the dodecapolar field (A_6), are of particular importance. The other higher-order fields are normally very small in weight and their effects are usually ignored. All the multiple expansion coefficients shown in this study were obtained by a least-square fit of Eq. (2) to the numerically calculated electric potential. As discussed earlier [33] the values given by this procedure are in good agreement with analytical solutions. For the ease of comparison between the strength of octapolar and dodecapolar fields, their percentage ratios to the quadrupolar field coefficient, $\%A_4/A_2$ and $\%A_6/A_2$, are used to represent their relative strengths.

It is well known that the end-cap holes and the truncation of the electrodes for a Paul trap add higher-order fields that cause undesirable effects such as delay of ion ejection [34] and deterioration of the mass resolution. This problem has been solved empirically by varying the geometry of the Paul trap in such a way as to adjust the distribution of the higher-order fields, mainly the octapolar and the dodecapolar fields, to give satisfactory mass analysis performance [33,34]. The additional resonances associated with these higher-order fields can cause undesirable ion loss, although they can also be exploited to improve ion trap performance. In some cases, the higher-order fields were used to improve the mass resolution by ejecting ions at the non-linear resonance points [46,47].

The simplified geometry of a CIT makes it easier to machine with appropriate tolerance, especially when this must be done on a small scale. Previous studies on the potential distribution inside the CIT show the field to be essentially quadrupolar in the central region [43,48,49]. However, the non-hyperbolic shape of the electrodes and the presence of end-cap holes introduce a large portion of negative dodecapolar field [15,18]. To compensate for the weakened strength of the field, the geometry of the CIT is usually adjusted to introduce a positive octapolar field to partially compensate for the negative higher-order field. In our experience, the best resolution of a CIT under the boundary or non-linear resonance ejection conditions is usually obtained when the sum of the relative strengths for the positive octapolar field and the negative dodecapolar field is about −10%. We have been using this "−10% compensation" rule as an empirical standard for the optimization of the CITs including the half size (r_0 = 5.0 mm) [16] and the quarter size (r_0 = 2.5 mm) devices [15]. In the general optimization process we recommend, the CIT geometry is altered until this empirical "−10% compensation" is achieved for the calculated field, and the performance of the CIT is verified by simulation before an actual device is fabricated.

3.2. Critical geometrical parameters and general optimization methodology

The geometrical parameters of the CIT are illustrated in Fig. 1 and it is expected that changing any of these parameters would cause a variation in the electric field strength inside the CIT. The geometry of CIT-0 as listed in Table 1 has been shown to give optimum performance [19]. Using the CIT-0 geometry as the basis, variations in the quadrupolar (A_2), octapolar (A_4) and dodecapolar (A_6) field contributions are calculated for a 10% increase of each geometrical parameter of the CIT-0. As shown in Table 2, the changes in field strength associated with changes in the dimensions r_0, z_b and d_s are much greater than those produced by changes in r_H, r_b and d_E. Therefore, r_0, z_b and d_s are regarded as the most critical geometrical parameters in the CIT optimization process. However, in actual the miniaturization of the CIT, the end-cap hole size is usually reduced more slowly than the trap radius to allow adequate transfer of electrons or ions, often so that the relative hole size is enlarged by 100% or more in the smaller instruments [15]. Hence, the end-cap hole size for the CIT must be considered as one of the major parameters during the CIT optimization via changing geometrical parameters.

Table 2
Percentage variation of the multipole expansion coefficients with 10% change in geometrical parameters[a] for CIT-0

Geometric parameters	$\%A_2$	$\%A_4$	$\%A_6$
r_0	14.93	−114.91	23.12
z_b	−11.11	68.55	−19.18
d_s	−4.60	10.10	−8.27
r_H	−0.03	−0.55	0.39
r_b	0.00	0.07	−0.02
d_E	0.00	0.08	−0.03

[a] The geometrical parameter z_0 is varied by 6.8% with 10% change of z_b, and 3.2% with 10% change of d_s.

In the initial non-optimized CIT geometry, some of these geometrical parameters are preset based on other requirements in the instrument design, normally including the maximum rf voltage for a certain mass range, which determines the ring electrode radius r_0, and the transfer efficiency of the ions or electrons, which determines the end-cap hole radius r_H. The optimization to the initial CIT geometry is then restricted to variation of the other critical geometrical parameters, z_b and d_s, until the "−10%" compensation value is achieved for the CIT internal electric field.

Generally, once an optimized geometry is found for a CIT of certain size, smaller CITs with optimized geometry, in terms of the electric fields, can be obtained by decreasing the geometric parameters in proportion. This approach is expected to provide similar analytical performance for smaller ion traps, except for effects of the smaller ion numbers [11]. However, this proportional shrinking method does not work well in practice due to the limitations imposed by other instrumental considerations. For instance, changes in the relative hole size can cause degradation in CIT performance. When no other changes were made to the geometry of CIT-0 except that the end-cap hole radius was increased from 0.5 to 1.5 mm, a new CIT geometry, CIT-1, was generated. An analyzer was fabricated with the CIT-1 geometry and the experimental test showed that its analytical resolution is worse than that of CIT-

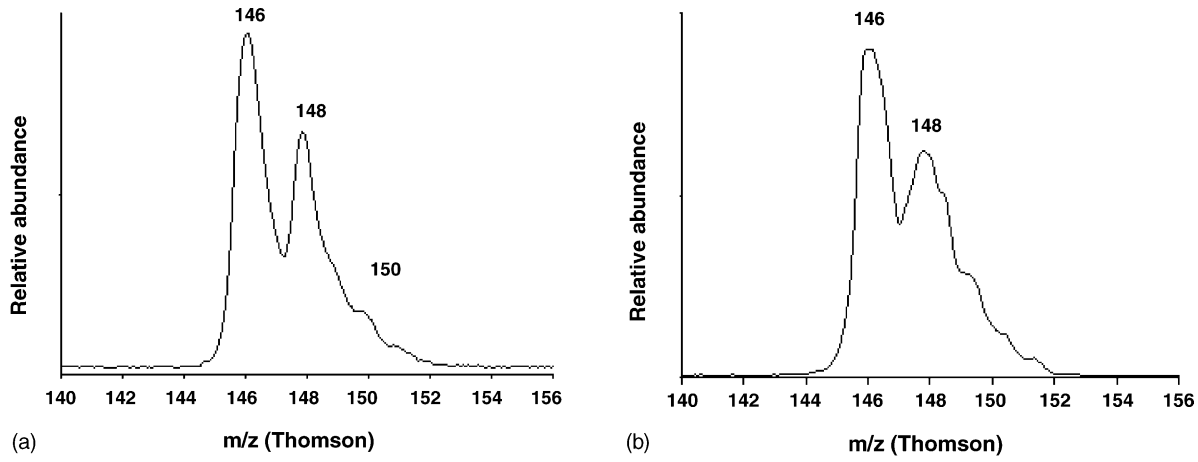

Fig. 3. Mass spectra (partial) of 1,3-dichlorobenzene collected under boundary ejection conditions for: (a) CIT-0 and (b) CIT-1. $P_{1,3\text{-dichlorobenzene}} = 8 \times 10^{-7}$, $P_{He} = 8 \times 10^{-5}$ Torr and rf frequency = 1.1 MHz.

0 (Fig. 3), as expected. Two isotope peaks at *m*/*z* 146 and 148 from 1,3-dichlorobenzene can be separated with a 40.9% valley for CIT-0 (Fig. 3a) and 55.2% valley for CIT-1 (Fig. 3b) with boundary ejection and a driving rf frequency = 1.1 MHz. A higher mass resolution can be achieved by using higher rf frequencies and non-linear resonance ejection [19].

The difference in the resolution obtained for CIT-0 and -1 can also be illustrated via a quantitative comparison of their electrical fields using the plots E_z versus z/z_0 and ΔE_z versus z/z_0 (Fig. 4) [33], where E_z is the axial field strength inside the CIT along the *z*-axis, while ΔE_z is the field strength contributed only by the non-linear fields. Both E_z and ΔE_z are expressed as fractions of the ideal quadrupolar field strength. In comparison with a pure quadrupolar field in an ideal quadrupole ion trap, the electric fields for CIT-0 and -1 both drop in the area close to the end-cap holes, which is a result of the existence of negative non-linear higher-order fields. This kind of decrease in the field strength is known to cause oscillation of the amplitude of the ion trajectory during the rf ramping intended to cause ion ejection. The resulting delay in ion ejection results in mass shifts and deterioration of the spectral resolution [34]. Compensation of the field can be achieved by adding positive higher-order fields through geometry optimization. A positive compensation to the electric field by a non-linear field component is found for CIT-0 but not for CIT-1 (Fig. 4b), which explains the difference in the resolution for these two CITs.

Given a geometry of a non-optimized CIT, such as CIT-1, the relative octapolar and dodecapolar field strengths can be easily calculated and the desirable changes to the field components can be obtained by comparison using the rough "−10% compensation" criterion. To reverse engineer the CIT geometry and make the sum of the relative strengths of the octapolar and dodecapolar fields approach −10%, the effects of the critical geometrical parameters were systematically studied. The CIT-0 geometry was used as the basis of the field calculation and each critical parameter was varied; the corresponding changes of the quadrupolar, octapolar and dodecapolar field components were calculated and are plotted as functions of the geometrical parameters (Fig. 5). Other CIT geometries have been used for this field calculation and it was found that though the values of the field components (A_2, $\%A_4/A_2$, $\%A_6/A_2$, $\%A_4/A_2 + \%A_6/A_2$) vary depending on the CIT geometry used, the trends of the variation as a function of the parameter variations are similar. These trends for the field change are instructive in terms of desirable changes that can be made to the geometrical parameters to increase or decrease the magnitudes of particular field components.

3.3. Geometry optimization

As listed in Table 3, the optimized CIT-0 geometry corresponds to a ($\%A_4/A_2 + \%A_6/A_2$) value of −10.3% while the non-optimized CIT-1 geometry corresponds to

Table 3
Multipole expansion coefficients for different CIT geometries

CIT	A_2 quadrupole	A_4 ($\%A_4/A_2$) octapole	A_6 ($\%A_6/A_2$) dodecapole	$\%A_4/A_2 + \%A_6/A_2$
CIT-0	0.736	0.055 (7.47%)	−0.131 (−17.80%)	−10.33
CIT-1	0.714	0.027 (3.78%)	−0.162 (−22.69%)	−18.91
CIT-2	0.646	0.068 (10.53%)	−0.130 (−20.12%)	−9.59
CIT-3	0.622	0.050 (8.04%)	−0.117 (−18.81%)	−10.77
CIT-4	0.692	0.086 (12.43%)	−0.157 (−22.69%)	−10.26

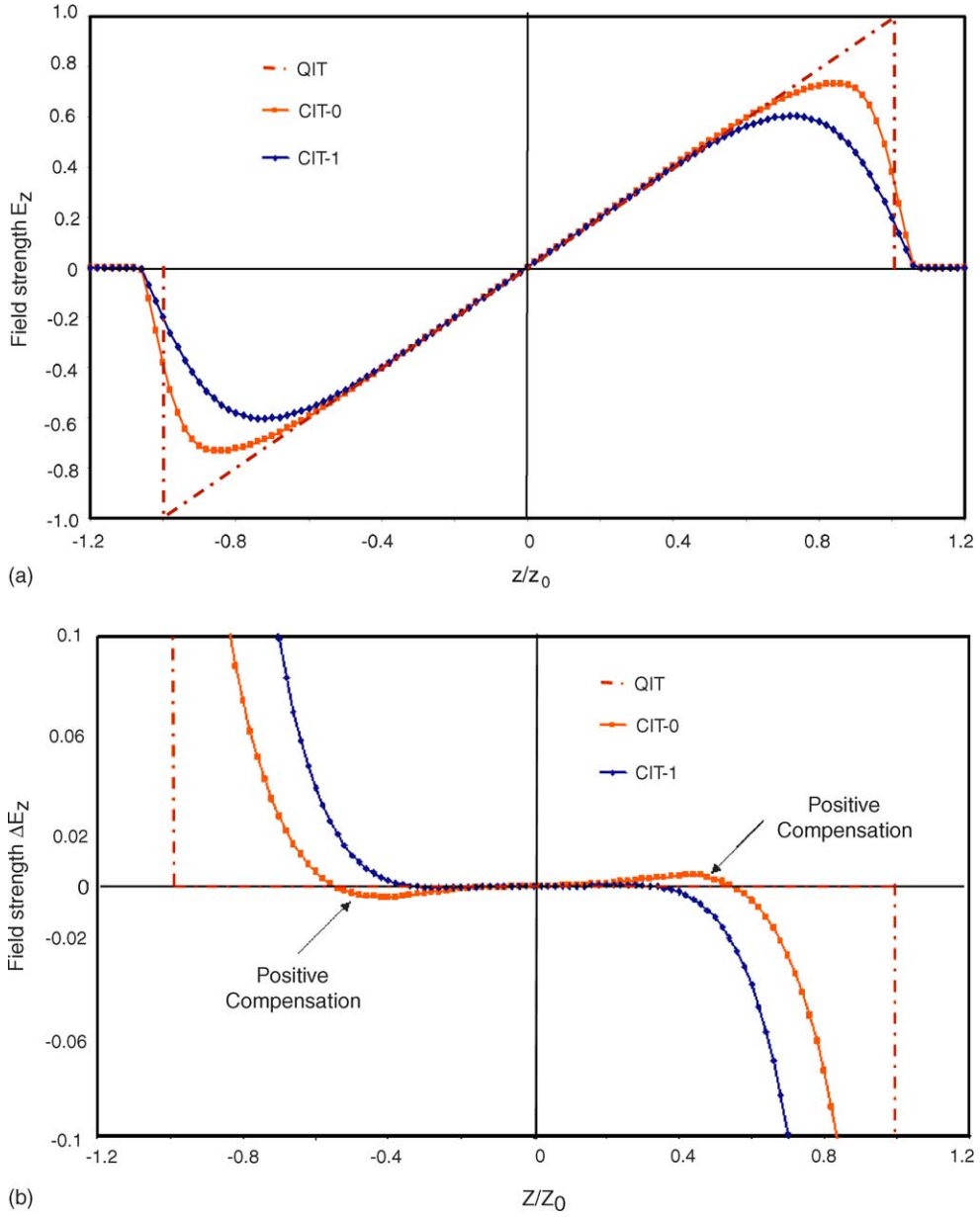

Fig. 4. (a) Axial electric field (E_z) and (b) non-linear contribution to the axial electric field (ΔE_z) along the z-axis in CIT-0 and -1 both with $r_0 = 5.0$ mm. Both fields are scaled independently with respect to the maximum value for each geometry and are expressed as fractions of the ideal quadrupolar field.

a ($\%A_4/A_2 + \%A_6/A_2$) value of −18.9%. Optimization of the CIT-1 geometry involves a process of varying the geometric parameters to increase the A_4 and A_6 contributions individually or collectively so the sum of the relative strengths ($\%A_4/A_2 + \%A_6/A_2$) is ca. −10%. To determine which parameters can be altered to provide such a field, the charts in Fig. 6 were used to identify the appropriate changes. If the large hole size of $r_H = 1.5$ mm is preferred for the purpose of maximizing signal, the ($\%A_4/A_2 + \%A_6/A_2$) value is expected to increase if (i) the half thickness of the ring electrode z_b is increased (CIT-2), (ii) the spacer d_s is increased (CIT-3), or (iii) the value z_b is increased and d_s is decreased while keeping $z_0 = 5.0$ mm constant (CIT-4). The electric fields for these three options were calculated for various changes and the $\%A_4/A_2$, $\%A_6/A_2$ and ($\%A_4/A_2 + \%A_6/A_2$) values are plotted in Fig. 6a–c as functions of each type of change. Using the "−10%" compensation rule as the criterion, the optimized geometries from these three different optimization methods were selected as listed in Table 1 and their higher-order fields are listed in Table 3.

Fig. 7 shows plots of E_z versus z/z_0 and ΔE_z versus z/z_0 for all five CIT geometries. In comparison with CIT-1, geometries of CIT-2, -3 and -4 have improved linearity in the axial electric field. More importantly, positive compensations were implemented for CIT-2, -3 and -4, with some differ-

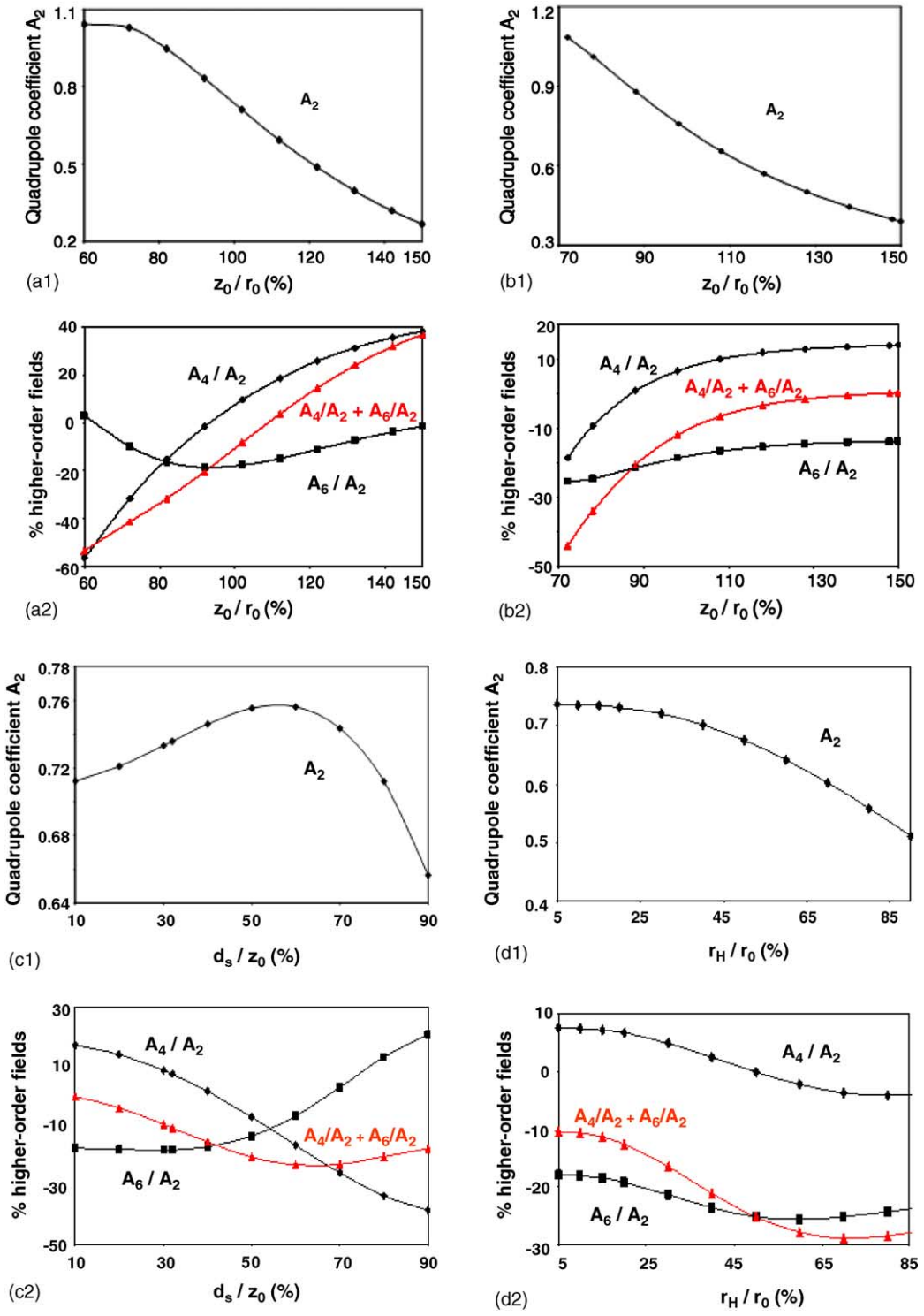

Fig. 5. Quadrupolar field (A_2), percentage of octapolar field (%A_4/A_2), percentage of dodecapolar field (%A_6/A_2) and field summation (%A_4/A_2 + %A_6/A_2) as functions of variation in CIT geometric parameters with inner radius r_0 = 5.0 mm: (a) z_b and spacer d_s = 1.6 mm, (b) spacer d_s and z_b = 3.4 mm, (c) z_b and spacer d_s simultaneously, to keep z_0 = 5.0 mm, (d) hole radius r_H. The potentials were calculated by using the Poisson/Superfish software package.

ences from the values used for CIT-0. These compensations were introduced using the various ways of optimizing the geometry of CIT-1 and are expected to improve the mass resolution.

3.4. Verification via simulations and experiments

The expected improved performance of the CITs with optimized geometries (CIT-2, -3 and -4) was verified first

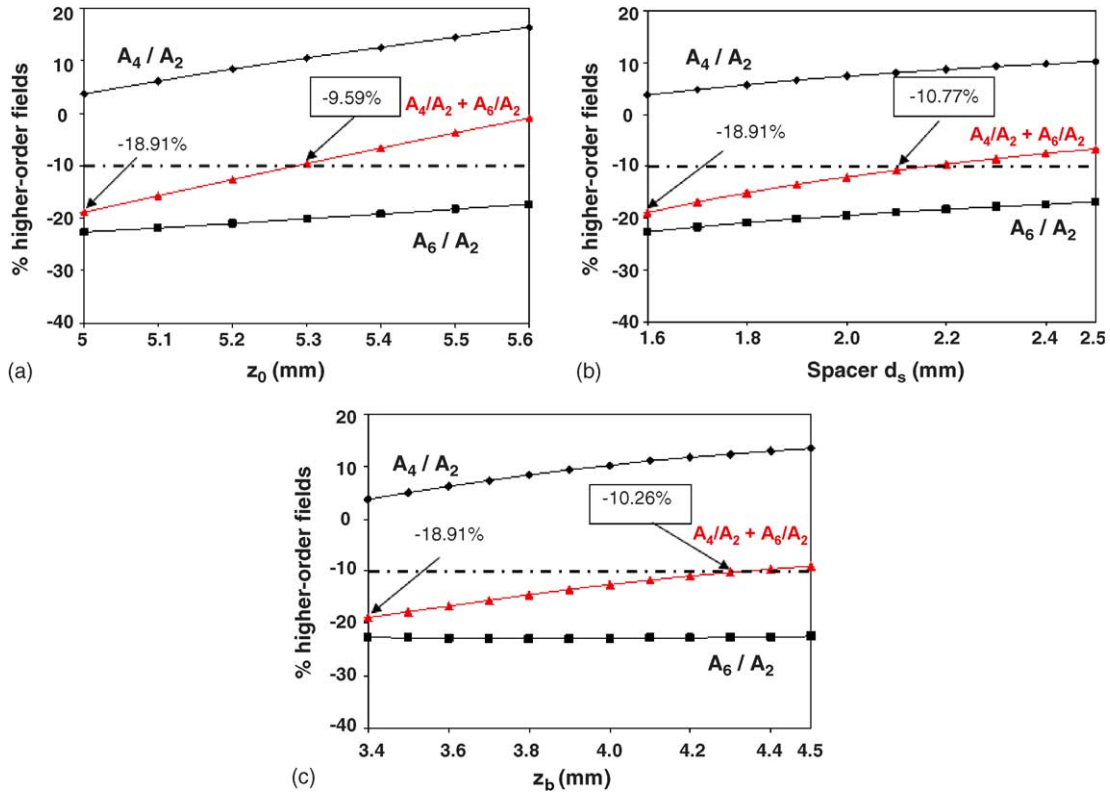

Fig. 6. Geometry optimization for CIT-1 (r_0 = 5.0 mm, z_0 = 5.0 mm, r_H = 1.5 mm) according to the "−10% Rule". Percentage of octapolar field (%A_4/A_2), percentage of dodecapolar field (%A_6/A_2) and field summation (%A_4/A_2 + %A_6/A_2) are plotted as functions of three CIT geometric parameters: (a) z_b, (b) spacer d_s, (c) z_b and spacer d_s simultaneously, to keep z_0 constant. The fields were calculated using the Poisson/Superfish software package.

with simulations. The trajectory calculations were performed using the ion trap simulation program ITSIM 5.0 (Purdue University, West Lafayette) and mass spectra for 1,3-dichlorobenzene were simulated under both boundary and resonance ejection conditions. Groups of ions were first generated that match the mass/charge ratio and the relative abundance of the fragment ions from 1,3-dichlorobenzene standard EI mass spectrum [50]. The generated ions had the same initial Gaussian distribution in space and zero initial velocity. A hard-sphere collision cross section of 50 Å^2 was assumed for each of the ions. Only elastic collisions were considered. The multiple ion trajectories were calculated by solving Newton's equation with fourth order Runge–Kutta method. A fixed integration step size (1/200 rf cycle = 4.5 ns) was chosen to provide sufficient accuracy for the simulations. The hybrid sum collision model, a combination of hard sphere and Langevin collision cross section, with random-angle-scattering was implemented to simulate ion–helium interactions at a temperature of 300 K. Space charge effects were not taken into account in the simulations since the ionization time in the experiment was controlled to limit the number of ions generated inside the CIT to avoid space charge effects. The applied voltages were defined in the form of scan tables, as done in early commercial ion traps. Scan tables are available for rf, ac, dc voltages and for arbitrary waveforms. The rf frequency was 1.1 MHz and the scan rate was 68 V/ms for the mass-selective instability scan (boundary ejection) and was previously calibrated for these experimental conditions. The calculation of the trajectory for each ion is terminated when the ion hits the trap electrodes or reaches a detector and the conditions are stored and used to generate mass spectra.

Boundary ejection is the most fundamental operation mode for ion traps, since the rf is applied to the ring electrode while both endcaps grounded. The rf voltage is increased in amplitude with time to scan the ions out of the trap. Due to their simplicity, mass spectra acquired using boundary ejection are often investigated first to give the intrinsic properties of the trap geometry. Fig. 8a shows the simulated isotope peaks *m/z* 146, 148 and 150 from 1,3-dichlorobenzene under boundary ejection conditions for the three optimized CIT geometries (CIT-2, -3 and –4). They all give better resolution of the isotope peaks compared with the non-optimized geometry CIT-1. The two peaks *m/z* 146 and 148 can be separated with 13.4% valley for CIT-2, 37.5% for CIT-3 and 25.8% for CIT-4. This kind of improvement in the simulated mass resolution indicates the success of optimization of the CIT geometry by each of the strategies. Experimental confirmation of this result is the last step required to complete the cycle and this is shown in Fig. 8b. The shape of the collected mass spectra and the mass resolution of the three isotope peaks are consistent with the simulation predictions. From the exper-

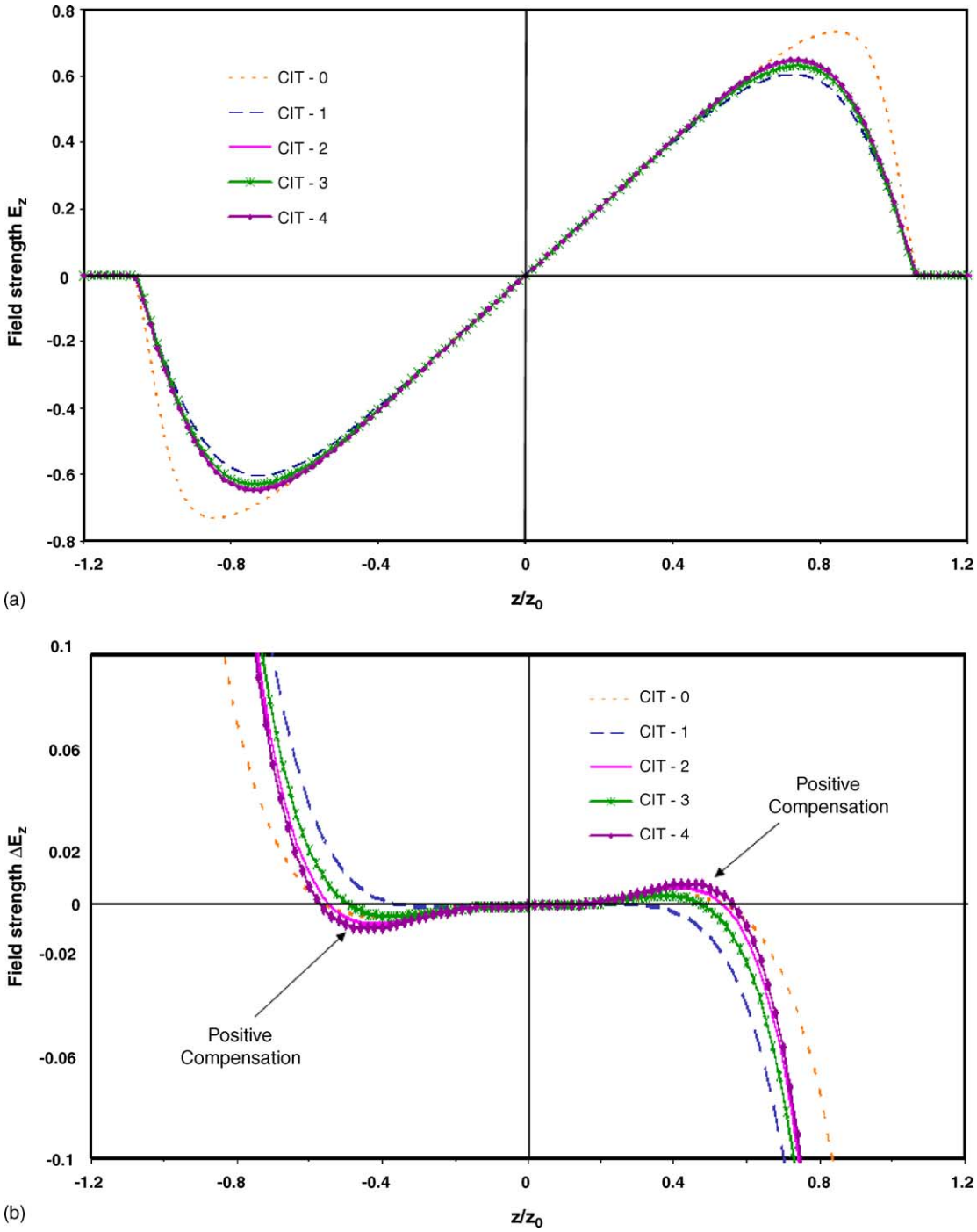

Fig. 7. (a) Axial electric field (E_z) and (b) non-linear contribution to the axial electric field (ΔE_z) along the z-axis in the different CITs (CIT-0, -1, -2, -3, -4) with both $r_0 = 5.0$ mm. Both fields are scaled independently with respect to the maximum value for each geometry and are expressed as fractions of the ideal quadrupolar field.

Fig. 8. Isotopic peaks $m/z = 146$, 148, 150 in the mass spectrum of 1,3-dichlorobenzene collected under boundary ejection conditions for three optimized CIT geometries (CIT-2, -3, -4) with inner radius $r_0 = 5.0$ mm and $r_H = 1.5$ mm. $P_{1,3\text{-dichlorobenzene}} = 8 \times 10^{-7}$, $P_{He} = 8 \times 10^{-5}$ Torr and rf frequency = 1.1 MHz: (a) mass spectra simulated under the same experimental conditions by using ion trap simulation program ITSIM 5.0 and (b) experimentally recorded mass spectra.

Fig. 9. Isotopic peaks $m/z = 146$, 148, 150 from mass spectra of 1,3-dichlorobenzene collected at resonance point $\beta_z = 0.9$ for three optimized CIT geometries (CIT-2, -3, -4) with inner radius $r_0 = 5.0$ mm and $r_H = 1.5$ mm. $P_{1,3\text{-dichlorobenzene}} = 8 \times 10^{-7}$, $P_{He} = 8 \times 10^{-5}$ Torr and rf frequency = 1.1 MHz. CIT-2: resonance ac frequency = 516 kHz, 900 $mV_{0\text{-p}}$, CIT-3: resonance ac frequency = 516 kHz, 620 $mV_{0\text{-p}}$, CIT-4: resonance ac frequency = 516 kHz, 400 $mV_{0\text{-p}}$: (a) mass spectra simulated under the same experimental conditions by using ion trap simulation program ITSIM 5.0 and (b) experimentally collected mass spectra.

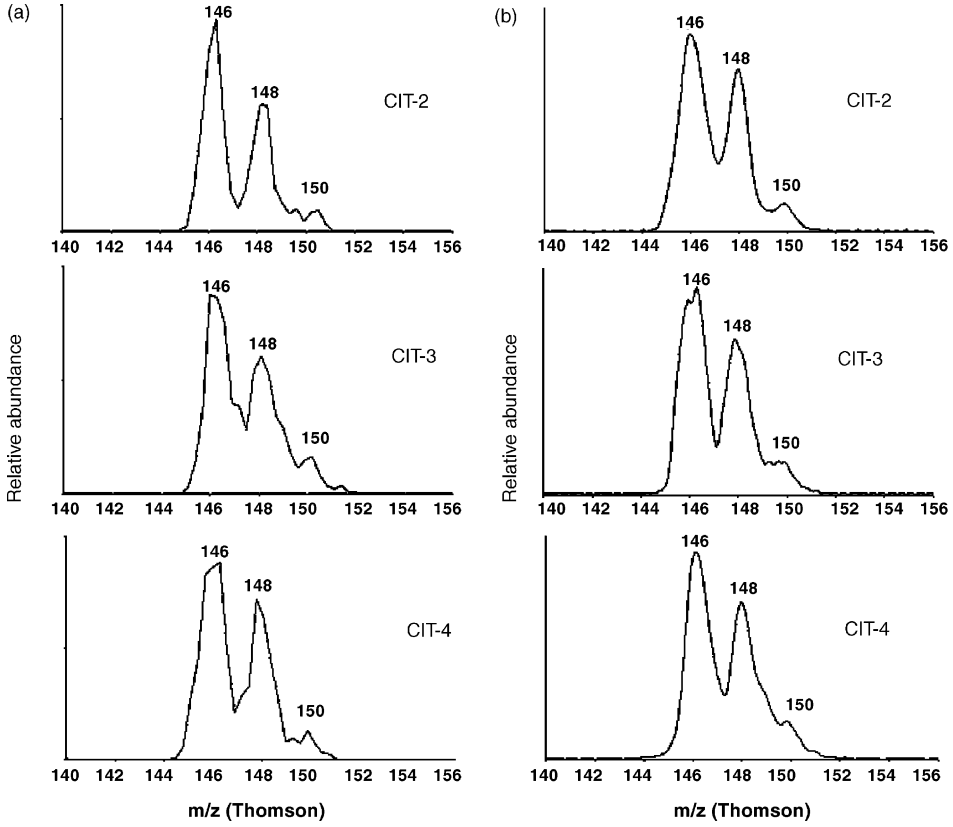
(a)
(b)
CIT-2
CIT-3
CIT-4
146
148
150
140 142 144 146 148 150 152 154 156
Relative abundance
m/z (Thomson)

Fig. 8.

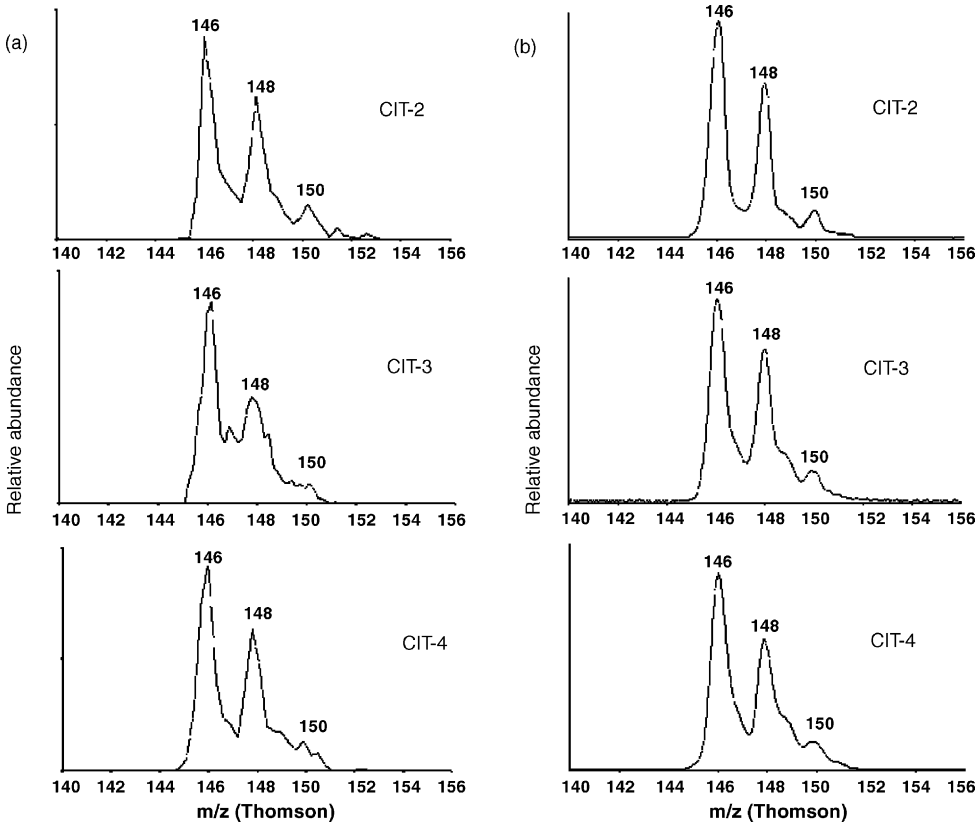
(a)
(b)
CIT-2
CIT-3
CIT-4
146
148
150
140 142 144 146 148 150 152 154 156
Relative abundance
m/z (Thomson)

Fig. 9.

iments, the two peaks at *m*/*z* 146 and 148 can be separated at 38.5% valley for CIT-2, 27.4% for CIT-3 and 34.6% for CIT-4.

Resonance ejection is often used to increase mass resolution since ions pick up energy more rapidly and are more tightly bunched as they are ejected from the trap. In both the simulation and experimental tests of the performance of the CITs with optimized geometries (CIT-2, -3 and -4) under resonance ejection conditions, a supplementary resonance ac signal with 516 kHz frequency ($\beta_z = 0.9$) and 180° phase difference was applied to the two end-cap electrodes. It is expected that the mass spectra collected using resonance ejection will have better mass resolution compared with boundary ejection [27]. Fig. 9a and b shows the spectra from simulation and experiments, respectively. Compared with the spectra (Fig. 8) collected using boundary ejection, the resonance ejection experiment does give better resolving power. The two peaks *m*/*z* 146 and 148 can be separated at 21.2% (simulation) and 15.6% (experiment) valley for CIT-2, 39.0% (simulation) and 23.3% (experiment) for CIT-3 and 19.1% (simulation) and 21.6% (experiment) for CIT-4.

3.5. Further performance improvements using non-linear resonance ejection

As discussed earlier in this paper, non-linear resonances can also be used to improve the mass resolution. The CITs with their geometries optimized for the boundary or resonance ejection at $\beta_z = 0.9$ do not necessarily give the best resolution at particular non-linear resonance ejection conditions. The "−10%" compensation rule might not apply for the optimized geometry for non-linear resonance ejection so the appropriate field distribution was explored further. Here, we can use ITSIM simulations to predict the performance under non-linear resonance conditions for CITs optimized for boundary and resonance ejection at $\beta_z = 0.9$ through the procedure described above and pick the one best suited for the construction of a non-linear ejection instrument. For CIT-2, -3 and -4, two ac signals with around 400 kHz frequency

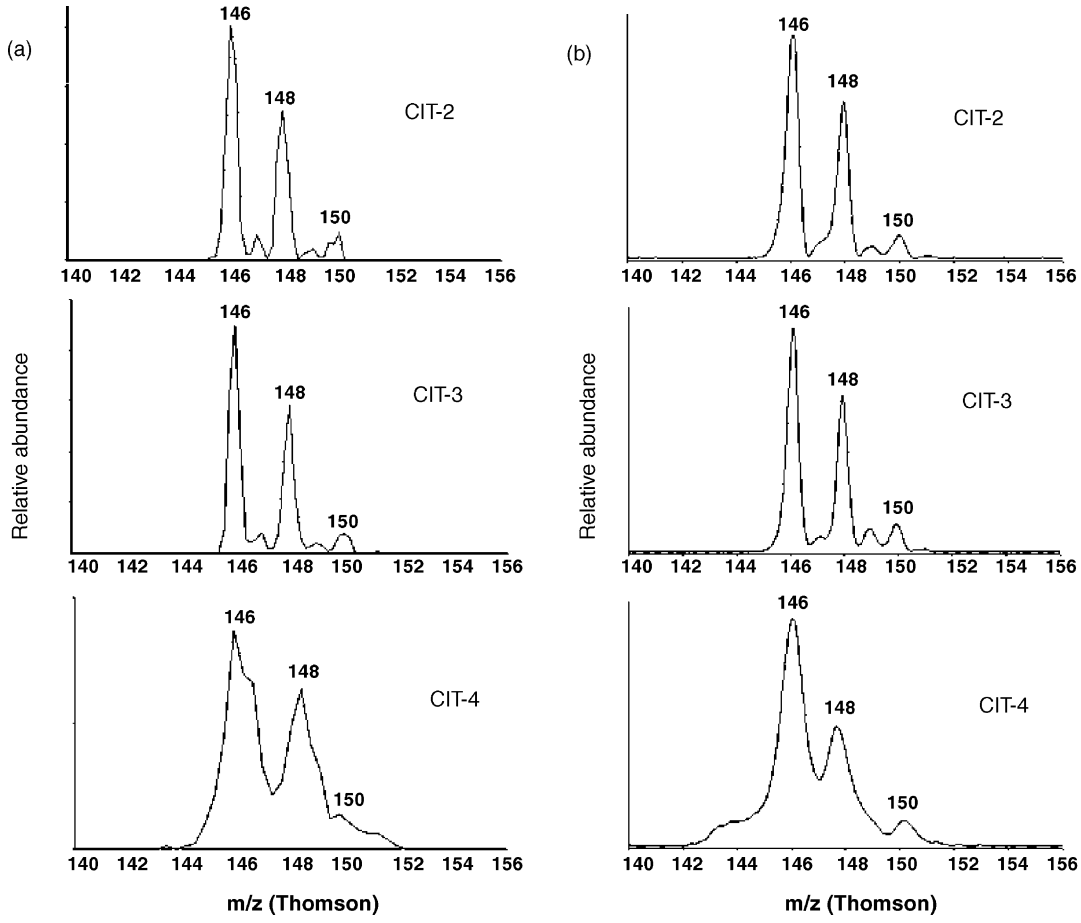

Fig. 10. Isotopic peaks *m*/*z* = 146, 148, 150 from mass spectra of 1,3-dichlorobenzene collected under non-linear resonance ejection conditions ($\beta_z = 0.7$) for three optimized CIT geometries (CIT-2, -3, -4) with inner radius $r_0 = 5.0$ mm and $r_H = 1.5$ mm. $P_{1,3\text{-dichlorobenzene}} = 8 \times 10^{-7}$, $P_{He} = 8 \times 10^{-5}$ Torr and rf frequency = 1.1 MHz. CIT-2: resonance ac frequency = 413 kHz, 1.2 $V_{0\text{-p}}$, CIT-3: resonance ac frequency = 400 kHz, 1.1 $V_{0\text{-p}}$, CIT-4: resonance ac frequency = 402 kHz, 700 m$V_{0\text{-p}}$: (a) mass spectra simulated under the same experimental conditions by using ion trap simulation program ITSIM 5.0 and (b) experimentally collected mass spectra.

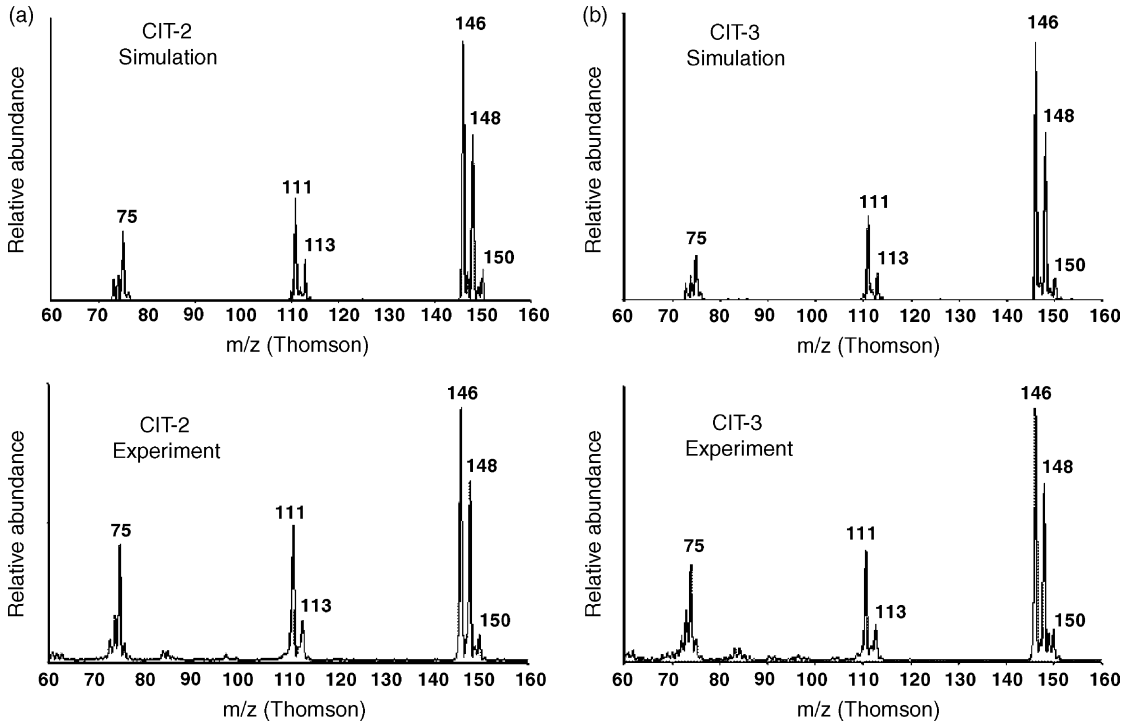

Fig. 11. Full mass spectra of 1,3-dichlorobenzene collected under non-linear-resonance ejection conditions ($\beta_z = 0.7$) for three optimized CIT geometries (a) CIT-2 and (b) CIT-3 with inner radius $r_0 = 5.0$ mm and $r_H = 1.5$ mm. $P_{1,3\text{-dichlorobenzene}} = 8 \times 10^{-7}$, $P_{He} = 8 \times 10^{-5}$ Torr and rf frequency = 1.1 MHz. CIT-2: resonance ac frequency = 413 kHz, 1.2 $V_{0\text{-p}}$, CIT-3: resonance ac frequency = 400 kHz, 1.1 $V_{0\text{-p}}$. Mass spectra were simulated under the same experimental conditions by using ion trap simulation program ITSIM 5.0.

($\beta_z = 0.7$, octapolar resonance point) and 180° difference in phase were applied to the end-cap electrodes for tests by simulation and experiment. Fig. 10 shows both the simulated and experimental spectra, again restricting the comparison to the ions *m*/*z* 146, 148 and 150 of 1,3-dichlorobenzene. The devices CIT-2 and -3 provided much better resolution than CIT-4, and baseline resolution was obtained for CIT-2 and -3. Trap CIT-4 has a relative strength of the octapolar field component that is larger than those for CIT-2 and -3, which indicates that an excessive octapolar field may degrade the resolution of ejection at an octapolar non-linear resonance point. The two peaks *m*/*z* 146 and 148 can only be separated at 28.2% (simulation) and 38.7% (experiment) valley for CIT-4. For non-linear resonance experiments, CIT-2 and -3 are the two best CIT optimized geometries. The full mass spectra of 1,3-dichlorobenzene collected via both simulation and experiment using these two CITs are shown in Fig. 11. These data demonstrate both the improvement in performance that can be achieved by appropriate geometry optimization and the good agreement of resolution between simulation and experiment.

4. Conclusions

The optimization of the electric field in a CIT can be achieved using the method described here, which includes the following steps:

- Step 1: select the initial geometrical parameters according to preferences which are set by other requirements in the instrument design;
- Step 2: calculate the electric field contributions associated with the initial CIT geometry, and compare with a set of standard electric field charts (as in Fig. 4) to determine how the parameters need to be varied;
- Step 3: adjust the parameters (r_0, z_b, d_s and r_H), calculate the electric fields and repeat this process until an appropriate distribution of components of the electric field is obtained. Here, we suggest the "-10%" compensation for positive octapolar and negative dodecapolar fields as a criterion for the appropriate field distribution for the boundary or linear resonance ejection mass scan experiments;
- Step 4: use the ion trap simulation (ITSIM) program to simulate the performance of the CIT with adjusted parameters to verify the improvement in performance;
- Step 5: fabricate a CIT with the optimized geometry and use it to record mass spectra for comparison with the simulated data.

The program ITSIM has been demonstrated to be a reliable tool for predicting the performance of CITs with various geometries and a valid approach to verify the optimization through field calculations. With further study and development, the optimization procedure described here can be extended for the optimization of other ion trap mass analyzers

with simple geometry, such as the rectilinear ion trap. The empirical criterion used in Step 3 for optimized field is a major subject of further tests and improvements for the CIT and other ion trap devices.

Acknowledgements

The authors acknowledge financial support from the US Department of Energy, Office of Basic Energy Science (DE-FG02-94ER14470). We also acknowledge Wolfgang R. Plass for valuable comments and discussions.

References

[1] J.A. Diaz, C.F. Giese, W.R. Gentry, Field Anal. Chem. Technol. 5 (2001) 156.
[2] J.A. Syage, B.J. Nies, M.D. Evans, K.A. Hanold, J. Am. Soc. Mass Spectrom. 12 (2001) 648.
[3] R.T. Short, D.P. Fries, M.L. Kerr, C.E. Lembke, S.K. Toler, P.G. Wenner, R.H. Byrne, J. Am. Soc. Mass Spectrom. 12 (2001) 676.
[4] B.A. Eckenrode, J. Am. Soc. Mass Spectrom. 12 (2001) 683.
[5] O.J. Orient, A. Chutjian, V. Garkanian, Rev. Sci. Instrum. 68 (1997) 1393.
[6] E.R. Badman, R.G. Cooks, J. Mass Spectrom. 35 (2000) 659.
[7] O.J. Orient, A. Chutjian, Rev. Sci. Instrum. 73 (2002) 2157.
[8] G. Miller, M. Koch, J.P. Hsu, F. Ozuna, Proceedings of the 45th ASMS Conference on Mass Spectrometry and Allied Topics, Palm Springs, CA, 1997.
[9] O. Kornienko, P.T.A. Reilly, W.B. Whitten, J.M. Ramsey, Rev. Sci. Instrum. 70 (1999) 3907.
[10] N. Sillon, R. Baptist, Sens. Actuators B 83 (2002) 129.
[11] M.G. Blain, L.S. Riter, D. Cruz, D.E. Austin, G. Wu, W.R. Plass, R.G. Cooks, Int. J. Mass Spectrom. 236 (2004) 91.
[12] E.R. Badman, R.G. Cooks, Anal. Chem. 72 (2000) 3291.
[13] E.R. Badman, R.C. Johnson, W.R. Plass, R.G. Cooks, Anal. Chem. 70 (1998) 4896.
[14] L.S. Riter, Y. Peng, R.J. Noll, G.E. Patterson, T. Aggerholm, R.G. Cooks, Anal. Chem. 74 (2002) 6154.
[15] E.R. Badman, Ph.D. Thesis, Purdue University, 2000.
[16] G. Wu, Z. Ouyang, W.R. Plass, R.G. Cooks, Proceedings of the 50th ASMS Conference on Mass Spectrometry and Allied Topics, Orlando, FL, 2002.
[17] D.B. Langmuir, R.V. Langmuir, H. Shelton, R.F. Wuerker, US Patent 3,065,640 (1962).
[18] J.M. Wells, E.R. Badman, R.G. Cooks, Anal. Chem. 70 (1998) 438.
[19] Z. Ouyang, E.R. Badman, R.G. Cooks, Rapid Commun. Mass Spectrom. 13 (1999) 2444.
[20] G.E. Patterson, A.J. Guymon, L.S. Riter, M. Everly, J. Griep-Raming, B.C. Laughlin, Z. Ouyang, R.G. Cooks, Anal. Chem. 74 (2002) 6145.
[21] Z. Ouyang, G. Wu, Y. Song, H. Li, W.R. Plass, R.G. Cooks, Anal. Chem. 76 (2004) 4595.
[22] A.M. Tabert, J. Griep-Raming, A.J. Guymon, R.G. Cooks, Anal. Chem. 75 (2003) 5656.
[23] P.H. Dawson, N.R. Whetten, J. Vac. Sci. Technol. 5 (1968) 1.
[24] J. Franzen, Int. J. Mass Spectrom. Ion Process. 106 (1991) 63.
[25] F.A. Londry, G.J. Wells, R.E. March, Rapid Commun. Mass Spectrom. 7 (1993) 43.
[26] M.W. Forbes, M. Sharifi, T. Croley, Z. Lausevic, R.E. March, J. Mass Spectrom. 34 (1999) 1219.
[27] J. Franzen, R.H. Gabling, M. Schubert, Y. Wang, in: R.E. March, J.F.J. Todd (Eds.), Practical Aspects of Ion Trap Mass Spectrometry, vol. 1, CRC Press, Boca Raton, FL, 1995 (Chapter 3).
[28] S. Sevugarajan, A.G. Menon, Int. J. Mass Spectrom. 197 (2000) 263.
[29] M. Sudakov, Int. J. Mass Spectrom. 206 (2001) 27.
[30] M.V. Dubkov, E.P. Sheretov, B.I. Kolotilin, M.P. Safonov, O.W. Rozhkov, E.V. Fedosov, Proceedings of the 50th ASMS Conference on Mass Spectrometry and Allied Topics, Orlando, FL, 2002.
[31] L. Ding, M. Sudakov, S. Kumashiro, Int. J. Mass Spectrom. 221 (2002) 117.
[32] M. Sudakov, D.J. Douglas, Rapid. Commun. Mass Spectrom. 17 (2003) 2290.
[33] W.R. Plass, Ph.D. Thesis, Justus-Liebig-Universität Giessen, Germany, 2001.
[34] W.R. Plass, H. Li, R.G. Cooks, Int. J. Mass Spectrom. 228 (2003) 237.
[35] S.A. Lammert, W.R. Plass, C.V. Thompson, M.B. Wise, Int. J. Mass Spectrom. 212 (2001) 25.
[36] H.A. Bui, R.G. Cooks, J. Mass Spectrom. 33 (1998) 297.
[37] J.H. Billen, L.M. Young, Proceedings of the 1993 Particle Accelator Conference, 1993, p. 790.
[38] P.H. Dawson (Ed.), Quadrupole Mass Spectrometry and Its Applications, Elsevier Scientific Publishing Co., New York, 1976.
[39] J.N. Louris, R.G. Cooks, J.E.P. Syka, P.E. Kelley, G.C. Stafford, J.F.J. Todd, Anal. Chem. 59 (1987) 1677.
[40] H.G. Dehmelt, Adv. Atom. Mol. Phys. 3 (1967) 53.
[41] J.D. Jakson, Classical Electrodynamics, 3rd ed., Wiley, 1999.
[42] M.N. Benilan, C. Audoin, Int. J. Mass Spectrom. Ion Phys. 11 (1973) 421.
[43] R.F. Bonner, J.E. Fulford, R.E. March, Int. J. Mass Spectrom. Ion Phys. 24 (1977) 255.
[44] W.H. Hartung, C.T. Avedisian, Proc. R. Soc. London A 437 (1992) 237.
[45] O. Kornienko, P.T.A. Reilly, W.B. Whitten, J.M. Ramsey, Rapid Commun. Mass Spectrom. 13 (1999) 50.
[46] Y. Wang, J. Franzen, K.P. Wanczek, Int. J. Mass Spectrom. Ion Process. 124 (1993) 125.
[47] Y. Wang, J. Franzen, Int. J. Mass Spectrom. Ion Process. 112 (1992) 167.
[48] H. Lagadec, C. Meis, M. Jardino, Int. J. Mass Spectrom. Ion Process. 85 (1988) 287.
[49] W. Lee, C. Oh, P. Kim, M. Yang, K. Song, Int. J. Mass Spectrom. 230 (2003) 25.
[50] http://webbook.nist.gov/chemistry/.